

Efficient and deterministic high-dimensional controlled-swap gates on hybrid linear optical systems with high fidelity

Gui-Long Jiang,¹ Jun-Bin Yuan,¹ Wen-Qiang Liu,² and Hai-Rui Wei^{1,*}

¹ School of Mathematics and Physics, University of Science and Technology Beijing, Beijing 100083, China

² Center for Quantum Technology Research and Key Laboratory of Advanced Optoelectronic Quantum Architecture and Measurements (MOE), School of Physics, Beijing Institute of Technology, Beijing 100081, China

Implementation of quantum logic gates with linear optical elements plays a prominent role in quantum computing due to the relatively easier manipulation and realization. We present efficient schemes to implement controlled-NOT (CNOT) gate and controlled-swap (Fredkin) gate by solely using linear optics. We encode the control qubits and target qudits in photonic polarization (two-level) and spatial degrees of freedom (d -level), respectively. Based on the hybrid encoding, CNOT and Fredkin gates are constructed in a deterministic way without any borrowed ancillary photons or measurement-induced nonlinearities. Remarkably, the number of linear optics required to implement a CNOT gate has been reduced to one polarization beam splitter (PBS), while only d PBSs are necessary to implement a generalized Fredkin gate. The optical depths of all schemes are reduced to one and dimension-independent. Besides, the fidelity of our three-qubit Fredkin gate is higher than 99.7% under realistic conditions, which is higher than the previous schemes.

PACS numbers: 03.67.Hk, 03.65.Ud, 03.67.Mn, 03.67.Pp

I. INTRODUCTION

Quantum computing has unparalleled advantages over classical computing in performing information-processing tasks [1–4], and it has the potential to solve certain discrete computational problems more efficiently; for example, Shor’s and Grover’s algorithms [5–8]. Universal quantum logic gates are the fundamental building blocks for a quantum computer [1, 2]. Among them, considerable attention has been paid to controlled-NOT (CNOT) gates, controlled-controlled-NOT (Toffoli) gates, and controlled-SWAP (CSWAP, Fredkin) gates. This is because arbitrary multiqubit quantum computation can be accurately simulated by CNOT gates and single-qubit rotations [2], and Fredkin and Toffoli gates form key ingredients of multiqubit unitary transformation [2], quantum algorithms [9], quantum cryptography [10, 11], and quantum fault tolerance [12]. Direct optical implementation of Fredkin and Toffoli gates is a more-efficient approach under realistic conditions, instead of synthesis programs [13–15] that are based on sequences of CNOT and Hadamard gates, leading to Fredkin and Toffoli gates being more susceptible to their environment.

CNOT and Fredkin gates have been experimentally demonstrated in various physical systems [16–18]. However, these candidates have certain weaknesses. For example, superconducting suffers from a short coherence time and weak scalability, the scalability of ion and high fidelity of neutral atom-based entangling gates is difficult to achieve experimentally, and spin in solids is challenged by inefficiency and impracticality. Compared with these complicated physical mediums, photonic qubits have sev-

eral advantages, such as negligible decoherence, diverse qubitlike degrees of freedom (DOFs) [19–22], and easy single-qubit operations with linear optical devices [23]. Moreover, the lack of interactions between individual photonic qubits has been remedied use of a cross-Kerr bus [24, 25] or linear-optics networks [26–30]. In particular, the architecture based on linear optics is the simplest to achieve with current technology, and linear optics-based schemes may be optimized use of high-dimensional Hilbert spaces [21] or multiple DOFs of a single photon [31, 32].

In high-dimensional quantum computing, blocks of these basic logic gates need to be arranged in order, which results in quantum circuits that are extremely complex and much low success probability. Integrated photonic circuits, based on a Mach-Zehnder interferometer (MZI) [33], might sidestep this obstacle [34–40]. By using path- or polarization-encoded qubits, such schemes enable large-scale quantum computations by decomposing arbitrary unitary transformations into multiple MZIs [33, 36, 41]. However, the imperfect linear optics and the higher number of paths make the fidelity of the quantum transformation low and make the gates more vulnerable to their environment. In contrast to constructions based on a single photonic DOF, constructions with multiple DOFs not only increase the capacity of the quantum information carried but also reduce the number of linear optics and transmission losses [31, 32]. Tremendous progress has been made with regard to deterministic quantum transformation with several photonic DOFs. Polarization-orbital-angular-momentum Toffoli and Fredkin gates were experimentally demonstrated in 2021 [42, 43]. In 2022, Meng [44] proposed a Fredkin gate based on polarization-entangled photon pairs with high fidelity. Chen *et al.* [45] optimized the unitary transformations in terms of a MZI and optical depth by using

*hrwei@ustb.edu.cn

in the $\{|000\rangle, |001\rangle, |010\rangle, |011\rangle, |100\rangle, |101\rangle, |110\rangle, |111\rangle\}$ basis.

The schematic setup, shown in Fig. 2(a), is designed to prepare the input normalization state $|\psi_{\text{in}}\rangle$ of the controlled-SWAP gate. Here

$$|\psi_{\text{in}}\rangle = (\alpha|1\rangle_1 + \beta|0\rangle_1) \otimes (\delta|1\rangle_2 + \gamma|0\rangle_2) \otimes (\nu|1\rangle_3 + \mu|0\rangle_3). \quad (11)$$

We first apply a spontaneous-parametric-down-conversion (SPDC) source to produce a polarization-entangled photon pair [46, 47]. After the pump pulse of the ultraviolet-light beam passes through two adjacent Type-I phase-matched β -barium borate (BBO) crystals, a two-photon pair will occupy spatial modes a and d with the normalization state

$$|\psi_{\text{initial}}\rangle = (\alpha\hat{a}_H^\dagger\hat{d}_H^\dagger + \beta\hat{a}_V^\dagger\hat{d}_V^\dagger)|\text{vac}\rangle. \quad (12)$$

Next, BS_1 and BS_2 are set to yield the transformations

$$\begin{aligned} \hat{a}_H^\dagger &\xrightarrow{\text{BS}_1} \gamma\hat{a}_H^\dagger + \delta\hat{b}_H^\dagger, & \hat{a}_V^\dagger &\xrightarrow{\text{BS}_1} \gamma\hat{a}_V^\dagger + \delta\hat{b}_V^\dagger, \\ \hat{d}_H^\dagger &\xrightarrow{\text{BS}_2} \mu\hat{c}_H^\dagger + \nu\hat{d}_H^\dagger, & \hat{d}_V^\dagger &\xrightarrow{\text{BS}_2} \mu\hat{c}_V^\dagger + \nu\hat{d}_V^\dagger, \end{aligned} \quad (13)$$

where $|\gamma|^2 + |\delta|^2 = |\mu|^2 + |\nu|^2 = 1$. Thus, BS_1 and BS_2 make $|\psi_{\text{initial}}\rangle$ change into

$$\begin{aligned} |\psi_{\text{in}}\rangle = & (\alpha\gamma\mu\hat{a}_H^\dagger\hat{c}_H^\dagger + \alpha\gamma\nu\hat{a}_H^\dagger\hat{d}_H^\dagger + \alpha\delta\mu\hat{b}_H^\dagger\hat{c}_H^\dagger \\ & + \alpha\delta\nu\hat{b}_H^\dagger\hat{d}_H^\dagger + \beta\gamma\mu\hat{a}_V^\dagger\hat{c}_V^\dagger + \beta\gamma\nu\hat{a}_V^\dagger\hat{d}_V^\dagger \\ & + \beta\delta\mu\hat{b}_V^\dagger\hat{c}_V^\dagger + \beta\delta\nu\hat{b}_V^\dagger\hat{d}_V^\dagger)|\text{vac}\rangle. \end{aligned} \quad (14)$$

This procedure is similar to the state preparation in Ref. [44]. By defining our logical qubits as

$$\begin{aligned} |VV\rangle &\equiv |0\rangle_1, & |HH\rangle &\equiv |1\rangle_1, \\ |a\rangle &\equiv |0\rangle_2, & |b\rangle &\equiv |1\rangle_2, \\ |c\rangle &\equiv |0\rangle_3, & |d\rangle &\equiv |1\rangle_3, \end{aligned} \quad (15)$$

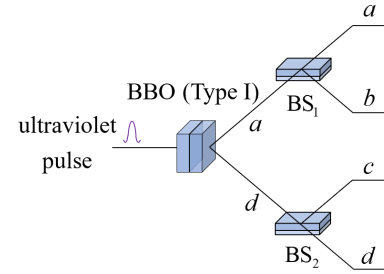
one can see that Eq. (14) corresponds to the general input state described in Eq. (11).

On the basis the encoding described above, the controlled-SWAP operation can be performed with the apparatus shown in Fig. 2(b). In detail, PBS_1 and PBS_2 induce the following transformations:

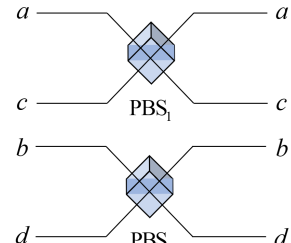
$$\begin{aligned} \hat{a}_V^\dagger &\xrightarrow{\text{PBS}_1} \hat{a}_V^\dagger, & \hat{a}_H^\dagger &\xrightarrow{\text{PBS}_1} \hat{c}_H^\dagger, \\ \hat{c}_V^\dagger &\xrightarrow{\text{PBS}_1} \hat{c}_V^\dagger, & \hat{c}_H^\dagger &\xrightarrow{\text{PBS}_1} \hat{a}_H^\dagger, \\ \hat{b}_V^\dagger &\xrightarrow{\text{PBS}_2} \hat{b}_V^\dagger, & \hat{b}_H^\dagger &\xrightarrow{\text{PBS}_2} \hat{d}_H^\dagger, \\ \hat{d}_V^\dagger &\xrightarrow{\text{PBS}_2} \hat{d}_V^\dagger, & \hat{d}_H^\dagger &\xrightarrow{\text{PBS}_2} \hat{b}_H^\dagger. \end{aligned} \quad (16)$$

Thus, PBS_1 and PBS_2 convert the state $|\psi_{\text{in}}\rangle$ described in Eq. (14) into

$$\begin{aligned} |\psi_{\text{out}}\rangle = & (\alpha\gamma\mu\hat{a}_H^\dagger\hat{c}_H^\dagger + \alpha\gamma\nu\hat{c}_H^\dagger\hat{b}_H^\dagger + \alpha\delta\mu\hat{d}_H^\dagger\hat{a}_H^\dagger \\ & + \alpha\delta\nu\hat{d}_H^\dagger\hat{b}_H^\dagger + \beta\gamma\mu\hat{a}_V^\dagger\hat{c}_V^\dagger + \beta\gamma\nu\hat{a}_V^\dagger\hat{d}_V^\dagger \\ & + \beta\delta\mu\hat{b}_V^\dagger\hat{c}_V^\dagger + \beta\delta\nu\hat{b}_V^\dagger\hat{d}_V^\dagger)|\text{vac}\rangle. \end{aligned} \quad (17)$$



(a) State preparation



(b) Controlled-swap gate

FIG. 2: (a) Experimental setup to create the input state of Fredkin gates. (b) The polarization-spatial controlled-SWAP gate with linear optics.

which corresponds to the output state

$$\begin{aligned} |\psi_{\text{out}}\rangle = & (\alpha\gamma\mu|100\rangle + \alpha\gamma\nu|110\rangle + \alpha\delta\mu|101\rangle \\ & + \alpha\delta\nu|111\rangle + \beta\gamma\mu|000\rangle + \beta\gamma\nu|001\rangle \\ & + \beta\delta\mu|010\rangle + \beta\delta\nu|011\rangle)_{123}. \end{aligned} \quad (18)$$

Therefore, only two PBSs is sufficient to implement a Fredkin gate, which is much less than 14 linear optics in Ref. [44].

C. The generalized controlled-SWAP gate on $\mathbb{C}^2 \otimes \mathbb{C}^3 \otimes \mathbb{C}^3$

We now extend the target system of controlled-SWAP gates to two three-dimensional Hilbert spaces $\mathbb{C}^3 \otimes \mathbb{C}^3$. The controlled-SWAP gate acting on the state in $\mathbb{C}^2 \otimes \mathbb{C}^3 \otimes \mathbb{C}^3$ can be described as

$$U_{\text{CSWAP}}^{2,3,3} = \sum_{i,j=0}^2 (|0ij\rangle\langle 0ij| + |1ij\rangle\langle 1ji|), \quad (19)$$

where $i, j = 0, 1, 2$.

The general input state of the gate $U_{\text{CSWAP}}^{2,3,3}$ can be generated by means of Fig. 3(a). As discussed in Sec. II B, a polarization-entangled photon pair $|\varphi_{\text{initial}}\rangle$ occupying spatial modes a and f can be generated by the SPDC source. Here

$$|\varphi_{\text{initial}}\rangle = (\alpha\hat{a}_H^\dagger\hat{f}_H^\dagger + \beta\hat{a}_V^\dagger\hat{f}_V^\dagger)|\text{vac}\rangle. \quad (20)$$

Subsequently, the two photons pass through the BS pairs (BS₁, BS₂) and (BS₃, BS₄) in succession. Here BS₁, BS₂, BS₃, and BS₄ complete the transformations

$$\begin{aligned} \hat{a}_\Gamma^\dagger &\xrightarrow{\text{BS}_1} x_1 \hat{a}_\Gamma^\dagger + y_1 \hat{c}_\Gamma^\dagger, & \hat{f}_\Gamma^\dagger &\xrightarrow{\text{BS}_2} x_2 \hat{d}_\Gamma^\dagger + y_2 \hat{f}_\Gamma^\dagger, \\ \hat{a}_\Gamma^\dagger &\xrightarrow{\text{BS}_3} x_3 \hat{a}_\Gamma^\dagger + y_3 \hat{b}_\Gamma^\dagger, & \hat{f}_\Gamma^\dagger &\xrightarrow{\text{BS}_4} x_4 \hat{e}_\Gamma^\dagger + y_4 \hat{f}_\Gamma^\dagger, \end{aligned} \quad (21)$$

where $\Gamma \in \{H, V\}$, and $|x_k|^2 + |y_k|^2 = 1$ ($k = 1, 2, 3, 4$). Hence, the operations transform the state $|\varphi_{\text{initial}}\rangle$ into

$$\begin{aligned} |\varphi_{\text{in}}\rangle = & (\theta_{100} \hat{a}_H^\dagger \hat{d}_H^\dagger + \theta_{101} \hat{a}_H^\dagger \hat{e}_H^\dagger + \theta_{102} \hat{a}_H^\dagger \hat{f}_H^\dagger \\ & + \theta_{110} \hat{b}_H^\dagger \hat{d}_H^\dagger + \theta_{111} \hat{b}_H^\dagger \hat{e}_H^\dagger + \theta_{112} \hat{b}_H^\dagger \hat{f}_H^\dagger \\ & + \theta_{120} \hat{c}_H^\dagger \hat{d}_H^\dagger + \theta_{121} \hat{c}_H^\dagger \hat{e}_H^\dagger + \theta_{122} \hat{c}_H^\dagger \hat{f}_H^\dagger \\ & + \theta_{000} \hat{a}_V^\dagger \hat{d}_V^\dagger + \theta_{001} \hat{a}_V^\dagger \hat{e}_V^\dagger + \theta_{002} \hat{a}_V^\dagger \hat{f}_V^\dagger \\ & + \theta_{010} \hat{b}_V^\dagger \hat{d}_V^\dagger + \theta_{011} \hat{b}_V^\dagger \hat{e}_V^\dagger + \theta_{012} \hat{b}_V^\dagger \hat{f}_V^\dagger \\ & + \theta_{020} \hat{c}_V^\dagger \hat{d}_V^\dagger + \theta_{021} \hat{c}_V^\dagger \hat{e}_V^\dagger + \theta_{022} \hat{c}_V^\dagger \hat{f}_V^\dagger) |\text{vac}\rangle. \end{aligned} \quad (22)$$

with

$$\begin{aligned} \theta_{100} &= \alpha x_1 x_2 x_3, & \theta_{101} &= \alpha x_1 y_2 x_3 x_4, \\ \theta_{102} &= \alpha x_1 y_2 x_3 y_4, & \theta_{110} &= \alpha x_1 x_2 y_3, \\ \theta_{111} &= \alpha x_1 y_2 y_3 x_4, & \theta_{112} &= \alpha x_1 y_2 y_3 y_4, \\ \theta_{120} &= \alpha y_1 x_2, & \theta_{121} &= \alpha y_1 y_2 x_4, \\ \theta_{122} &= \alpha y_1 y_2 y_4, & \theta_{000} &= \beta x_1 x_2 x_3, \\ \theta_{001} &= \beta x_1 y_2 x_3 x_4, & \theta_{002} &= \beta x_1 y_2 x_3 y_4, \\ \theta_{010} &= \beta x_1 x_2 y_3, & \theta_{011} &= \beta x_1 y_2 y_3 x_4, \\ \theta_{012} &= \beta x_1 y_2 y_3 y_4, & \theta_{020} &= \beta y_1 x_2, \\ \theta_{021} &= \beta y_1 y_2 x_4, & \theta_{022} &= \beta y_1 y_2 y_4. \end{aligned} \quad (23)$$

On the basis of the encoding rules

$$\begin{aligned} |VV\rangle &\equiv |0\rangle_1, |HH\rangle \equiv |1\rangle_1, \\ |a\rangle &\equiv |0\rangle_2, \quad |b\rangle \equiv |1\rangle_2, \quad |c\rangle \equiv |2\rangle_2, \\ |d\rangle &\equiv |0\rangle_3, \quad |e\rangle \equiv |1\rangle_3, \quad |f\rangle \equiv |2\rangle_3, \end{aligned} \quad (24)$$

one can see that Eq. (22) corresponds to the general input logical state

$$\begin{aligned} |\varphi_{\text{in}}\rangle = & (\theta_{100} |100\rangle + \theta_{101} |101\rangle + \theta_{102} |102\rangle \\ & + \theta_{110} |110\rangle + \theta_{111} |111\rangle + \theta_{112} |112\rangle \\ & + \theta_{120} |120\rangle + \theta_{121} |121\rangle + \theta_{122} |122\rangle \\ & + \theta_{000} |000\rangle + \theta_{001} |001\rangle + \theta_{002} |002\rangle \\ & + \theta_{010} |010\rangle + \theta_{011} |011\rangle + \theta_{012} |012\rangle \\ & + \theta_{020} |020\rangle + \theta_{021} |021\rangle + \theta_{022} |022\rangle)_{123}. \end{aligned} \quad (25)$$

We note that Eq. (25) is just the expanded version of the general input state on $\mathbb{C}^2 \otimes \mathbb{C}^2 \otimes \mathbb{C}^2$ described in Eq.(11).

On the basis of Eq. (22) and Eq. (24), $U_{\text{CSWAP}}^{2,3,3}$ can be efficiently constructed by use of three PBSs as shown

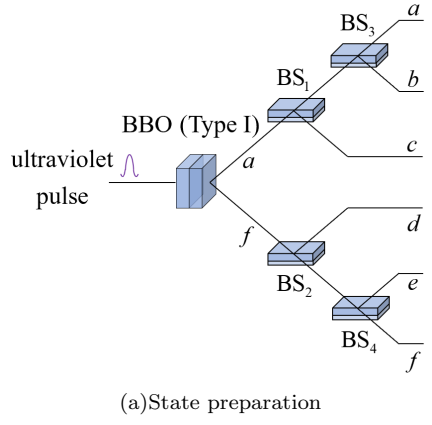


FIG. 3: (a) Experimental setup of the state preparation. (b) The linear-optical controlled-SWAP gate on $\mathbb{C}^2 \otimes \mathbb{C}^3 \otimes \mathbb{C}^3$.

in Fig. 3(b), where the PBSs result in

$$\begin{aligned} \hat{a}_V^\dagger &\xrightarrow{\text{PBS}_1} \hat{a}_V^\dagger, & \hat{a}_H^\dagger &\xrightarrow{\text{PBS}_1} \hat{d}_H^\dagger, \\ \hat{d}_V^\dagger &\xrightarrow{\text{PBS}_1} \hat{d}_V^\dagger, & \hat{d}_H^\dagger &\xrightarrow{\text{PBS}_1} \hat{a}_H^\dagger, \\ \hat{b}_V^\dagger &\xrightarrow{\text{PBS}_2} \hat{b}_V^\dagger, & \hat{b}_H^\dagger &\xrightarrow{\text{PBS}_2} \hat{e}_H^\dagger, \\ \hat{e}_V^\dagger &\xrightarrow{\text{PBS}_2} \hat{e}_V^\dagger, & \hat{e}_H^\dagger &\xrightarrow{\text{PBS}_2} \hat{b}_H^\dagger, \\ \hat{c}_V^\dagger &\xrightarrow{\text{PBS}_3} \hat{c}_V^\dagger, & \hat{c}_H^\dagger &\xrightarrow{\text{PBS}_3} \hat{f}_H^\dagger, \\ \hat{f}_V^\dagger &\xrightarrow{\text{PBS}_3} \hat{f}_V^\dagger, & \hat{f}_H^\dagger &\xrightarrow{\text{PBS}_3} \hat{c}_H^\dagger. \end{aligned} \quad (26)$$

After the wavepackets have been mixed at PBS₁, PBS₂, and PBS₃, the initial state $|\varphi_{\text{in}}\rangle$ will be

$$\begin{aligned} |\varphi_{\text{out}}\rangle = & (\theta_{100} \hat{a}_H^\dagger \hat{d}_H^\dagger + \theta_{101} \hat{b}_H^\dagger \hat{d}_H^\dagger + \theta_{102} \hat{c}_H^\dagger \hat{d}_H^\dagger \\ & + \theta_{110} \hat{a}_H^\dagger \hat{e}_H^\dagger + \theta_{111} \hat{b}_H^\dagger \hat{e}_H^\dagger + \theta_{112} \hat{c}_H^\dagger \hat{e}_H^\dagger \\ & + \theta_{120} \hat{a}_H^\dagger \hat{f}_H^\dagger + \theta_{121} \hat{b}_H^\dagger \hat{f}_H^\dagger + \theta_{122} \hat{c}_H^\dagger \hat{f}_H^\dagger \\ & + \theta_{000} \hat{a}_V^\dagger \hat{d}_V^\dagger + \theta_{001} \hat{a}_V^\dagger \hat{e}_V^\dagger + \theta_{002} \hat{a}_V^\dagger \hat{f}_V^\dagger \\ & + \theta_{010} \hat{b}_V^\dagger \hat{d}_V^\dagger + \theta_{011} \hat{b}_V^\dagger \hat{e}_V^\dagger + \theta_{012} \hat{b}_V^\dagger \hat{f}_V^\dagger \\ & + \theta_{020} \hat{c}_V^\dagger \hat{d}_V^\dagger + \theta_{021} \hat{c}_V^\dagger \hat{e}_V^\dagger + \theta_{022} \hat{c}_V^\dagger \hat{f}_V^\dagger) |\text{vac}\rangle. \end{aligned} \quad (27)$$

which corresponds to the output state

$$\begin{aligned} |\varphi_{\text{out}}\rangle = & (\theta_{100}|100\rangle + \theta_{101}|110\rangle + \theta_{102}|120\rangle \\ & + \theta_{110}|101\rangle + \theta_{111}|111\rangle + \theta_{112}|121\rangle \\ & + \theta_{120}|102\rangle + \theta_{121}|112\rangle + \theta_{122}|122\rangle \\ & + \theta_{000}|000\rangle + \theta_{001}|001\rangle + \theta_{002}|002\rangle \\ & + \theta_{010}|010\rangle + \theta_{011}|011\rangle + \theta_{012}|012\rangle \\ & + \theta_{020}|020\rangle + \theta_{021}|021\rangle + \theta_{022}|022\rangle)_{123}. \end{aligned} \quad (28)$$

D. The generalized controlled-SWAP gate on $\mathbb{C}^2 \otimes \mathbb{C}^d \otimes \mathbb{C}^d$

The device in Fig. 3 can be extended to implement the controlled-SWAP gate $U_{\text{CSWAP}}^{2,d,d}$ on $\mathbb{C}^2 \otimes \mathbb{C}^d \otimes \mathbb{C}^d$, where

$$U_{\text{CSWAP}}^{2,d,d} = \sum_{i,j=0}^{d-1} (|0ij\rangle\langle 0ij| + |1ij\rangle\langle 1ji|), \quad (29)$$

where $i, j = 0, 1, 2, \dots, d-1$.

A similar argument as made in Sec. II C, Fig. 4(a) presents the expanded version of the input state. We suppose that $d = 2^n + q$, where $0 \leq q < 2^n$ and n is a positive integer. The SPDC source produces a polarization-entangled state

$$|\omega_{\text{initial}}\rangle = (\alpha \hat{a}_{0H}^\dagger \hat{b}_{0H}^\dagger + \beta \hat{a}_{0V}^\dagger \hat{b}_{0V}^\dagger) |\text{vac}\rangle, \quad (30)$$

in the spatial modes a_0 and b_0 .

Subsequently, the photon in the spatial path a_0 (b_0) is driven through BS_1 (BS_2), yielding spatial basis states $\{|a_0\rangle, |a_1\rangle\}$ ($\{|b_0\rangle, |b_1\rangle\}$). Next, BS_3 and BS_4 (BS_5 and BS_6) are set in paths $|a_0\rangle$ and $|a_1\rangle$ ($|b_0\rangle$ and $|b_1\rangle$) to generate four spatial basis states $\{|a_0\rangle, |a_1\rangle, |a_2\rangle, |a_3\rangle\}$ ($\{|b_0\rangle, |b_1\rangle, |b_2\rangle, |b_3\rangle\}$). The triangular array of BSs is expanded until the 2^n spatial basis states $\{|a_0\rangle, |a_1\rangle, \dots, |a_{2^n-1}\rangle\}$ ($\{|b_0\rangle, |b_1\rangle, \dots, |b_{2^n-1}\rangle\}$) are obtained.

Finally, q BSs are set to q spatial modes of $\{a_0, a_1, \dots, a_{2^n-1}\}$ separately to produce d spatial basis states $\{|a_0\rangle, |a_1\rangle, \dots, |a_{d-1}\rangle\}$, and for the same is done for $\{b_0, b_1, \dots, b_{2^n-1}\}$. Note that this step is not necessary if $q = 0$. Putting all the pieces together, one can see that $2(d-1)$ BSs are applied, and the state $|\omega_{\text{initial}}\rangle$ becomes

$$|\omega_{\text{in}}\rangle = \sum_{i,j=0}^{d-1} (\theta_{1ij} \hat{a}_{iH}^\dagger \hat{b}_{jH}^\dagger + \theta_{0ij} \hat{a}_{iV}^\dagger \hat{b}_{jV}^\dagger) |\text{vac}\rangle. \quad (31)$$

Here $\sum_{i,j=0}^{d-1} (|\theta_{1ij}|^2 + |\theta_{0ij}|^2) = 1$. The complex parameters θ_{0ij} and θ_{1ij} are determined by α , β , and reflection and transmission parameters of the $2(d-1)$ BSs.

If we encode the computing logic qubits as

$$\begin{aligned} |VV\rangle &\equiv |0\rangle_1, |HH\rangle \equiv |1\rangle_1, \\ |a_i\rangle &\equiv |i\rangle_2, \quad |b_j\rangle \equiv |j\rangle_3 (i, j = 0, 1, \dots, d-1). \end{aligned} \quad (32)$$

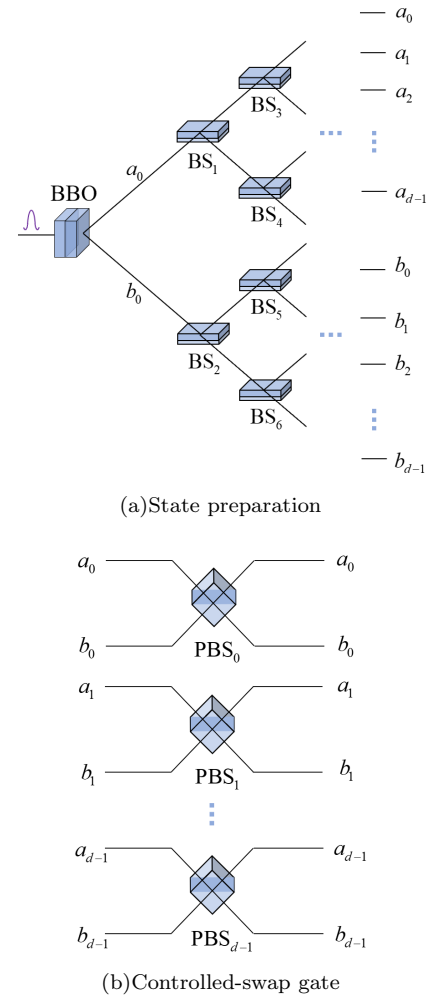


FIG. 4: (a) Experimental setup of the state-preparation. (b) The controlled-SWAP gate on $\mathbb{C}^2 \otimes \mathbb{C}^d \otimes \mathbb{C}^d$.

The input state of $U_{\text{CSWAP}}^{2,d,d}$ described in Eq. (31) corresponds to

$$|\omega_{\text{in}}\rangle = \sum_{i,j=0}^{d-1} (\theta_{1ij} |1ij\rangle + \theta_{0ij} |0ij\rangle). \quad (33)$$

As shown in Fig. 4(b), $U_{\text{CSWAP}}^{2,d,d}$ can be implemented by using solely d PBSs. Specifically, when the control logic qubit is in the state $|0\rangle_1$ corresponding to $|VV\rangle$, the spatial-based target states will not be changed by the PBSs, i.e.,

$$|0ij\rangle_{123} \xrightarrow{\text{PBSs}} |0ij\rangle_{123} (i, j = 0, 1, \dots, d-1). \quad (34)$$

When the control logic qubit is in the state $|1\rangle_1$ corresponding to $|HH\rangle$, the target states will be exchanged by the PBSs, i.e.,

$$\hat{a}_{iH}^\dagger \hat{b}_{jH}^\dagger \xrightarrow{\text{PBSs}} \hat{a}_{jH}^\dagger \hat{b}_{iH}^\dagger (i, j = 0, 1, \dots, d-1), \quad (35)$$

which corresponds to

$$|1ij\rangle_{123} \xrightarrow{\text{PBSs}} |1ji\rangle_{123} (i, j = 0, 1, \dots, d-1). \quad (36)$$

On the basis of Eqs. (34) and (36), it can be deduced that

$$|\omega_{\text{in}}\rangle \xrightarrow{\text{PBSs}} |\omega_{\text{out}}\rangle = \sum_{i,j=0}^{d-1} (\theta_{1ij}|1ji\rangle + \theta_{0ij}|0ij\rangle). \quad (37)$$

Therefore, only d PBSs can efficiently complete the operation $U_{\text{CSWAP}}^{2,2,d}$.

III. AVERAGE FIDELITY OF THE CONTROLLED-SWAP GATE

The schemes presented all are constructed by use of solely PBSs, and these PBSs can be replaced with calcite beam displacers (BDs) as they all essentially direct the photons into different spatial modes on the basis of the polarization states. To conveniently compare the performance in Fig. 2(b) with that of the scheme proposed in Ref. [44], we consider the imperfections induced by the PBS ($\bar{U}_{\text{PBS}}^\dagger$) to be the same as those induced by the calcite beam displacer ($\bar{U}_{\text{BD}}^\dagger$). That is, $\bar{U}_{\text{PBS}}^\dagger$ accomplishes the following transformations [44]:

$$\hat{\chi}_H^\dagger \xrightarrow{\bar{U}_{\text{PBS}}^\dagger} \frac{1}{\sqrt{1+|r|}} [(\cos\theta - \sqrt{r}\sin\theta)\hat{\eta}_H^\dagger - (\sin\theta + \sqrt{r^*}\cos\theta)\hat{\eta}_V^\dagger], \quad (38)$$

$$\hat{\eta}_H^\dagger \xrightarrow{\bar{U}_{\text{PBS}}^\dagger} \frac{1}{\sqrt{1+|r|}} [(\cos\theta - \sqrt{r}\sin\theta)\hat{\chi}_H^\dagger - (\sin\theta + \sqrt{r^*}\cos\theta)\hat{\chi}_V^\dagger], \quad (39)$$

$$\hat{\chi}_V^\dagger \xrightarrow{\bar{U}_{\text{PBS}}^\dagger} \frac{1}{\sqrt{1+|r|}} [(\sin\theta + \sqrt{r}\cos\theta)\hat{\chi}_H^\dagger + (\cos\theta - \sqrt{r^*}\sin\theta)\hat{\chi}_V^\dagger], \quad (40)$$

$$\hat{\eta}_V^\dagger \xrightarrow{\bar{U}_{\text{PBS}}^\dagger} \frac{1}{\sqrt{1+|r|}} [(\sin\theta + \sqrt{r}\cos\theta)\hat{\eta}_H^\dagger + (\cos\theta - \sqrt{r^*}\sin\theta)\hat{\eta}_V^\dagger], \quad (41)$$

where θ and r are the deviation of mirror mounts and the polarization extinction ratio of the PBS, respectively, $(\chi, \eta) = (a, c)$ or $(\chi, \eta) = (b, d)$, and $\sqrt{r^*}$ denotes the conjugate complex of \sqrt{r} .

The performance of the presented controlled-SWAP gate $U_{\text{CSWAP}}^{2,2,2}$ can be evaluated by

$$\begin{aligned} \bar{F} &= \frac{1}{(2\pi)^3} \int_0^{2\pi} \int_0^{2\pi} \int_0^{2\pi} |\langle \psi_{\text{real}} | \psi_{\text{out}} \rangle|^2 dx dy dz \\ &= \frac{(\cos\theta - \sqrt{r}\sin\theta)^4}{(1+|r|)^2} + \frac{3}{16} \cdot \frac{(\sin\theta + \sqrt{r}\cos\theta)^4}{(1+|r|)^2}, \end{aligned} \quad (42)$$

where the ideal output state $|\psi_{\text{out}}\rangle$ is given by Eq. (18) and $|\psi_{\text{real}}\rangle$ represents the practical output state with $\alpha =$

$\cos x$, $\beta = \sin x$, $\gamma = \cos y$, $\delta = \sin y$, $\mu = \cos z$, and $v = \sin z$. Figure 5 shows the average fidelity \bar{F} of $U_{\text{CSWAP}}^{2,2,2}$ as a function of r and θ . In particular, when $r = 0.001$ and $\theta = 0.005\text{rad}$, the average fidelity $\bar{F} = 0.997$.

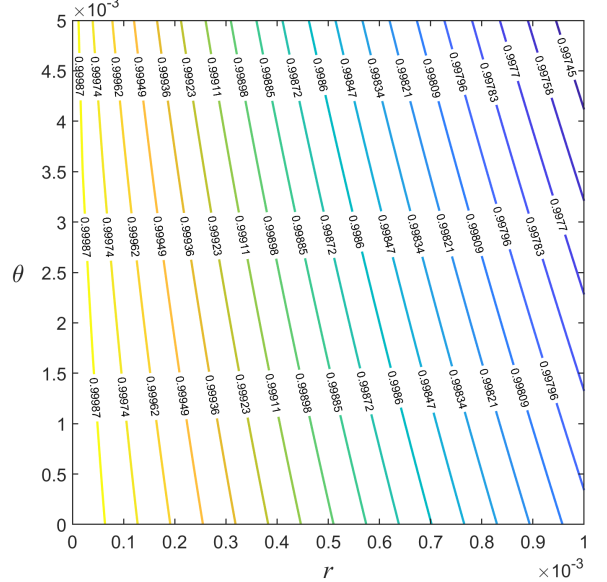


FIG. 5: Average fidelity \bar{F} of the controlled-SWAP gate $U_{\text{CSWAP}}^{2,2,2}$ with $r \in [0, 1 \times 10^{-3}]$ and $\theta \in [0, 5 \times 10^{-3}]$.

For the input state $|\psi'\rangle = |000\rangle$ of $U_{\text{CSWAP}}^{2,2,2}$ corresponding to $\hat{a}_V^\dagger \hat{c}_V^\dagger |vac\rangle$, the ideal output state $|\psi'_{\text{ideal}}\rangle$ and the practical $|\psi'_{\text{real}}\rangle$ can be calculated as

$$|\psi'_{\text{ideal}}\rangle = \hat{a}_V^\dagger \hat{c}_V^\dagger |vac\rangle, \quad (43)$$

$$\begin{aligned} |\psi'_{\text{real}}\rangle &= \frac{1}{1+|r|} [(\sin\theta + \sqrt{r}\cos\theta)^2 \hat{a}_H^\dagger \hat{c}_H^\dagger \\ &\quad + (\sin\theta + \sqrt{r}\cos\theta)(\cos\theta - \sqrt{r^*}\sin\theta) \hat{a}_H^\dagger \hat{c}_V^\dagger \\ &\quad + (\cos\theta - \sqrt{r^*}\sin\theta)(\sin\theta + \sqrt{r}\cos\theta) \hat{a}_V^\dagger \hat{c}_H^\dagger \\ &\quad + (\cos\theta - \sqrt{r^*}\sin\theta)^2 \hat{a}_V^\dagger \hat{c}_V^\dagger] |vac\rangle. \end{aligned} \quad (44)$$

Thus, the average fidelity of $U_{\text{CSWAP}}^{2,2,2}$ for the input state $|000\rangle$ is given by

$$\bar{F}_{000} = |\langle \psi'_{\text{real}} | \psi'_{\text{ideal}} \rangle|^2 = \left| \frac{(\cos\theta - \sqrt{r}\sin\theta)^2}{1+|r|} \right|^2. \quad (45)$$

It is easy to verify that $\bar{F}_{000} = \bar{F}_{001} = \bar{F}_{010} = \bar{F}_{011} = \bar{F}_{100} = \bar{F}_{101} = \bar{F}_{110} = \bar{F}_{111}$.

Figure 6 shows that \bar{F}_{000} is much greater than \mathcal{F}_{000} , \mathcal{F}_{001} , \mathcal{F}_{010} , \mathcal{F}_{011} , \mathcal{F}_{100} , \mathcal{F}_{101} , \mathcal{F}_{110} , and \mathcal{F}_{111} presented in Ref. [44]. Moreover,

$$\begin{aligned} \mathcal{F}_{000} &= \mathcal{F}_{001} = \mathcal{F}_{010} = \mathcal{F}_{011} \\ &= \left| \frac{(\cos\theta - \sqrt{r}\sin\theta)^2}{1+|r|} \right|^2 \times \left| \frac{1}{1+r} \right|^2, \end{aligned} \quad (46)$$

$$\begin{aligned} \mathcal{F}_{100} &= \mathcal{F}_{101} = \mathcal{F}_{110} = \mathcal{F}_{111} \\ &= \mathcal{F}_{000} \times \left| \left(\frac{i(1+\epsilon)(1-e^{i(\pi-\Delta\phi)})}{2+2\epsilon+\epsilon^2} \right)^4 \right|^2, \end{aligned} \quad (47)$$

where the imperfect parameters ϵ and $\Delta\phi$ are induced by BSs and phase shifters (PSs), respectively. Although the presented \bar{F}_{000} is slightly greater than \mathcal{F}_{000} and \mathcal{F}_{100} as shown in Fig. 6 (where $\epsilon = 0.02, \Delta\phi = \pi/36$, see Ref. [44]), \bar{F}_{000} is affected only by r and θ , whereas errors ϵ and $\Delta\phi$ are eliminated.

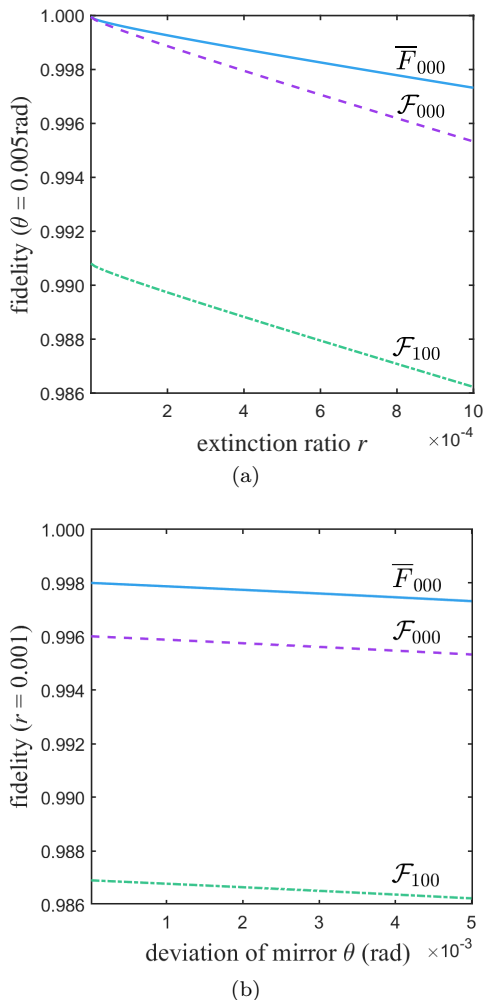


FIG. 6: (a) Fidelities of controlled-SWAP gate $U_{\text{CSWAP}}^{2,2,2}$ as a function of the extinction ratio r with $\theta = 5 \times 10^{-3}$ rad. (b) Fidelities of controlled-SWAP gate $U_{\text{CSWAP}}^{2,2,2}$ as a function of the deviation of mirror mounts θ with $r = 1 \times 10^{-3}$. The solid blue curves are for our \bar{F}_{00j} or \bar{F}_{10j} , the dashed purple curves are for \mathcal{F}_{00j} [44], and the dash-dotted green curves are for \mathcal{F}_{10j} [44], where $i, j \in (0, 1)$.

IV. DISCUSSION AND SUMMARY

Quantum logic gates are at the heart of quantum computing, and it has recently been demonstrated that use of multi-DOF encoding to implement quantum logic gates not only reduces the number of steps required to manipulate quantum states but also increases the fidelity of the logic gate [44, 45]. In this work, we design deterministic schemes for implementing a CNOT gate and a family of controlled-SWAP gates based on linear optics. The proposed schemes have several advantages over the synthesis-based one in Ref. [21], such as fewer linear optical elements and photonic resources, lower depth, and higher fidelity. The control qubit and the target qubit (qudits) of the CNOT (controlled-SWAP) gate are encoded in the polarization and spatial states of a single photon (an entangled photon pair), respectively.

TABLE I: Comparison of CNOT and controlled-SWAP gates with the gates reported in Ref. [44].

	Study	Linear optics	Number of elements	Depth
$U_{\text{CNOT}}^{2,2}$	Meng [44]	BD,BS,PS	5	5
	This work	PBS	1	1
$U_{\text{CSWAP}}^{2,2,2}$	Meng [44]	BD,BS,PS	14	11
	This work	PBS	2	1
$U_{\text{CSWAP}}^{2,d,d}$	Meng [44]	none	none	none
	This work	PBS	d	1

As shown in Table I, the presented CNOT gate $U_{\text{CNOT}}^{2,2}$ can be completed by use of one PBS, and the depth of the circuit is 1. The same work reported in Ref. [44] requires two BDs, two BSs, and one PS, and the optical depth is 5. Our three-qubit controlled-SWAP gate $U_{\text{CSWAP}}^{2,2,2}$ can be implemented with 2 PBSs, beating the earlier scheme of 14 linear optics [44]. The optical depth of 1 for the gate $U_{\text{CSWAP}}^{2,2,2}$ is much lower than 11 in Ref. [44]. Then we extend the program to $U_{\text{CSWAP}}^{2,d,d}$. Remarkably, the extended architecture requires d PBSs and the d -independent optical depth is 1. Moreover, the fidelity of $U_{\text{CSWAP}}^{2,2,2}$ shown in Fig. 6 is more than 99.7%, which is also slightly higher than 99% in Ref. [44], and the error can be further reduced by the quantum Zeno effect [48].

The presented schemes for linear optical control gates are effective and easy to achieve with current technology. With distinct merits of multi-DOF encoding, our effective hybrid schemes have strong potential for high-dimensional quantum computing and quantum communication.

ACKNOWLEDGEMENTS

This work was supported by the National Natural Science Foundation of China under Grant No. 62371038 and

the Fundamental Research Funds for the Central Universities under Grant No. FRF-TP-19-011A3.

[1] M. A. Nielsen and I. L. Chuang, *Quantum Computation and Quantum Information* (Cambridge University Press, Cambridge, 2000).

[2] A. Barenco, C. H. Bennett, R. Cleve, D. P. DiVincenzo, N. Margolus, P. Shor, T. Sleator, J. A. Smolin, and H. Weinfurter, Elementary gates for quantum computation, *Phys. Rev. A* **52**, 3457 (1995).

[3] T. Li and G. L. Long, Hyper-parallel optical quantum computation assisted by atomic ensemble embedded in double-sided optical cavities, *Phys. Rev. A* **94**, 022343 (2016).

[4] S. Bravyi, D. Gosset, and R. König, Quantum advantage with shallow circuits, *Science* **362**, 308 (2018).

[5] P. W. Shor, Polynomial-Time Algorithms for Prime Factorization and Discrete Logarithms on a Quantum Computer, *SIAM Rev.* **41**, 303 (1999).

[6] L. K. Grover, Quantum Mechanics Helps in Searching for a Needle in a Haystack, *Phys. Rev. Lett.* **79**, 325 (1997).

[7] G. L. Long, Grover algorithm with zero theoretical failure rate, *Phys. Rev. A* **64**, 022307 (2001).

[8] A. Politi, J. C. F. Matthews, and J. L. O'Brien, Shor's Quantum Factoring Algorithm on a Photonic Chip, *Science* **325**, 1221 (2009).

[9] E. Martín-López, A. Laing, T. Lawson, R. Alvarez, X. Q. Zhou, and J. L. O'Brien, Experimental realization of Shor's quantum factoring algorithm using qubit recycling, *Nat. Photonics* **6**, 773 (2012).

[10] H. Buhrman, R. Cleve, J. Watrous, and R. d. Wolf, Quantum Fingerprinting, *Phys. Rev. Lett.* **87**, 167902 (2001).

[11] B. Wang and L. M. Duan, Implementation scheme of controlled SWAP gates for quantum fingerprinting and photonic quantum computation, *Phys. Rev. A* **75**, 050304(R) (2007).

[12] J. Guillaud and M. Mirrahimi, Repetition Cat Qubits for Fault-Tolerant Quantum Computation, *Phys. Rev. X* **9**, 041053 (2019).

[13] J. A. Smolin and D. P. DiVincenzo, Five two-bit quantum gates are sufficient to implement the quantum Fredkin gate, *Phys. Rev. A* **53**, 2855 (1996).

[14] N. Yu, R. Duan, and M. Ying, Five two-qubit gates are necessary for implementing the Toffoli gate, *Phys. Rev. A* **88**, 010304(R) (2013).

[15] N. Yu and M. Ying, Optimal simulation of Deutsch gates and the Fredkin gate, *Phys. Rev. A* **91**, 032302 (2015).

[16] G. J. Milburn, Quantum Optical Fredkin Gate, *Phys. Rev. Lett.* **62**, 2124 (1989).

[17] J. I. Cirac and P. Zoller, Quantum Computations with Cold Trapped Ions, *Phys. Rev. Lett.* **74**, 4091 (1995).

[18] J. H. Plantenberg, P. C. de Groot, C. J. P. M. Harmans, and J. E. Mooij, Demonstration of controlled-NOT quantum gates on a pair of superconducting quantum bits, *Nature (London)* **447**, 836 (2007).

[19] H. H. Lu, J. M. Lukens, B. P. Williams, P. Imany, N. A. Peters, A. M. Weiner, and P. Lougovski, A controlled-NOT gate for frequency-bin qubits, *npj Quantum Inform.* **5**, 24 (2019).

[20] T. Li and G. L. Long, Quantum secure direct communication based on single-photon Bell-state measurement, *New J. Phys.* **22**, 063017 (2020).

[21] W. Q. Liu, H. R. Wei, and L. C. Kwek, Low-Cost Fredkin Gate with Auxiliary Space, *Phys. Rev. Appl.* **14**, 054057 (2020).

[22] Z. Xie, Y. Liu, X. Mo, T. Li, and Z. Li, Quantum entanglement creation for distant quantum memories via time-bin multiplexing, *Phys. Rev. A* **104**, 062409 (2021).

[23] B. N. Simon, C. M. Chandrashekhar, and S. Simon, Hamilton's turns as a visual tool kit for designing single-qubit unitary gates, *Phys. Rev. A* **85**, 022323 (2012).

[24] Q. Lin and J. Li, Quantum control gates with weak cross-Kerr nonlinearity, *Phys. Rev. A* **79**, 022301 (2009).

[25] X. W. Wang, D. Y. Zhang, S. Q. Tang, L. J. Xie, Z. Y. Wang, and L. M. Kuang, Photonic two-qubit parity gate with tiny cross-Kerr nonlinearity, *Phys. Rev. A* **85**, 052326 (2012).

[26] E. Knill, R. Laflamme, and G. J. Milburn, A scheme for efficient quantum computation with linear optics, *Nature (London)* **409**, 46 (2001).

[27] J. L. O'Brien, G. J. Pryde, A. Gilchrist, D. F. V. James, N. K. Langford, T. C. Ralph, and A. G. White, Quantum Process Tomography of a Controlled-NOT Gate, *Phys. Rev. Lett.* **93**, 080502 (2004).

[28] R. Okamoto, H. F. Hofmann, S. Takeuchi, and K. Sasaki, Demonstration of an Optical Quantum Controlled-NOT Gate without Path Interference, *Phys. Rev. Lett.* **95**, 210506 (2005).

[29] J. Fiurášek, Linear-optics quantum Toffoli and Fredkin gates, *Phys. Rev. A* **73**, 062313 (2006).

[30] Y. X. Gong, G. C. Guo, and T. C. Ralph, Methods for a linear optical quantum Fredkin gate, *Phys. Rev. A* **78**, 012305 (2008).

[31] I. Dhand and S. K. Goyal, Realization of arbitrary discrete unitary transformations using spatial and internal modes of light, *Phys. Rev. A* **92**, 043813 (2015).

[32] D. Su, I. Dhand, L. G. Helt, Z. Vernon, and K. Brádler, Hybrid spatiotemporal architectures for universal linear optics, *Phys. Rev. A* **99**, 062301 (2019).

[33] M. Reck, A. Zeilinger, H. J. Bernstein, and P. Bertani, Experimental realization of any discrete unitary operator, *Phys. Rev. Lett.* **73**, 58 (1994).

[34] J. Zeuner, A. N. Sharma, M. Tillmann, R. Heilmann, M. Gräfe, A. Moqanaki, A. Szameit, and P. Walther, Integrated-optics heralded controlled-NOT gate for polarization-encoded qubits, *npj Quantum Inform.* **4**, 13 (2018).

[35] W. Bogaerts, D. Pérez, J. Capmany, D. A. B. Miller, J. Poon, D. Englund, F. Morichetti, and A. Melloni, Programmable photonic circuits, *Nature (London)* **586**, 207 (2020).

[36] M. Y. Saygin, I. V. Kondratyev, I. V. Dyakonov, S. A. Mironov, S. S. Straupe, and S. P. Kulik, Robust Architecture for Programmable Universal Unitaries, *Phys. Rev. Lett.* **124**, 010501 (2020).

[37] M. Zhang, L. Feng, M. Li, Y. Chen, L. Zhang, D. He,

G. Guo, G. Guo, X. Ren, and D. Dai, Supercompact Photonic Quantum Logic Gate on a Silicon Chip, *Phys. Rev. Lett.* **126**, 130501 (2021).

[38] J. M. Arrazola, V. Bergholm, K. Brádler, T. R. Bromley, M. J. Collins, I. Dhand, A. Fumagalli, T. Gerrits, A. Goussev, L. G. Helt, J. Hundal, T. Isacsson, R. B. Israel, J. Izaac, S. Jahangiri, R. Janik, N. Killoran, S. P. Kumar, J. Lavoie, A. E. Lita, D. H. Mahler, M. Menotti, B. Morrison, S. W. Nam, L. Neuhaus, H. Y. Qi, N. Quesada, A. Repington, K. K. Sabapathy, M. Schuld, D. Su, J. Swinerton, A. Száva, K. Tan, P. Tan, V. D. Vaidya, Z. Vernon, Z. Zabaneh, and Y. Zhang, Quantum circuits with many photons on a programmable nanophotonic chip, *Nature (London)* **591**, 54 (2021).

[39] Y. Li, L. Wan, H. Zhang, H. Zhu, Y. Shi, L. K. Chin, X. Zhou, L. C. Kwek, and A. Q. Liu, Quantum Fredkin and Toffoli gates on a versatile programmable silicon photonic chip, *npj Quantum Inform.* **8**, 112 (2022).

[40] Y. Chi, Y. Yu, Q. Gong, and J. Wang, High-dimensional quantum information processing on programmable integrated photonic chips, *Sci. China-Inf. Sci.* **66**, 180501 (2023).

[41] W. R. Clements, P. C. Humphreys, B. J. Metcalf, W. S. Kolthammer, and I. A. Walmsley, Optimal design for universal multiport interferometers, *Optica* **3**, 1460 (2016).

[42] S. Ru, Y. Wang, M. An, F. Wang, P. Zhang, and F. Li, Realization of a deterministic quantum Toffoli gate with a single photon, *Phys. Rev. A* **103**, 022606 (2021).

[43] F. Wang, S. Ru, Y. Wang, M. An, P. Zhang, and F. Li, Experimental demonstration of a quantum controlled-SWAP gate with multiple degrees of freedom of a single photon, *Quantum Sci. Technol.* **6**, 035005 (2021).

[44] H. Meng, Deterministic linear-optical quantum control gates utilizing path and polarization degrees of freedom, *Phys. Rev. A* **105**, 032607 (2022).

[45] D. X. Chen, J. Jia, P. Zhang, and C. P. Yang, Optimized architectures for universal quantum state transformations using photonic path and polarization, *Quantum Sci. Technol.* **8**, 015011 (2022).

[46] S. Y. Baek and Y. H. Kim, Spectral properties of entangled photon pairs generated via frequency-degenerate type-I spontaneous parametric down-conversion, *Phys. Rev. A* **77**, 043807 (2008).

[47] Yu-Bo Sheng, Fu-Guo Deng, and Hong-Yu Zhou, Efficient polarization-entanglement purification based on parametric down-conversion sources with cross-Kerr nonlinearity, *Phys. Rev. A* **77**, 042308 (2008).

[48] X. Y. Long, W. T. He, N. N. Zhang, K. Tang, Z. D. Lin, H. F. Liu, X. F. Nie, G. R. Feng, J. Li, T. Xin, Q. Ai, and D. W. Lu, Entanglement-Enhanced Quantum Metrology in Colored Noise by Quantum Zeno Effect, *Phys. Rev. Lett.* **129**, 070502 (2022).